Available online at www.sciencedirect.com
ScienceDirect
Journal of Sound and Vibration 311 (2008) 1004–1019
JOURNAL OF SOUND AND VIBRATION
www.elsevier.com/locate/jsvi

Vibration control of vehicle ER suspension system using fuzzy moving sliding mode controller

Kum-Gil Sung, Young-Min Han, Jae-Wan Cho, Seung-Bok Choi*

Smart Structures and Systems Laboratory, Department of Mechanical Engineering, Inha University, Incheon 402-751, Republic of Korea

Received 27 December 2006; received in revised form 19 June 2007; accepted 28 September 2007
Available online 5 November 2007

Abstract

This paper presents robust vibration control performances of an electrorheological (ER) suspension system subjected to parameter uncertainty. A cylindrical type of ER damper is designed and manufactured on the basis of the required damping force level for a middle-sized passenger vehicle, and its field-dependent damping force and dynamic characteristics are experimentally evaluated. The ER damper is then incorporated to a quarter vehicle suspension system which is composed of sprung mass, spring and tire. After formulating the governing equation of motion of the proposed ER suspension system with parameter variations, a new moving sliding mode controller (MSMC) is formulated by adopting the fuzzy logic for the moving algorithm. The fuzzy MSMC is then experimentally realized with the quarter vehicle for the demonstration of a practical feasibility. Control performances such as vertical displacement and acceleration are evaluated in time and frequency domains under various road conditions. In addition, in order to verify the effectiveness of the proposed control strategy a comparative work between the proposed controller and conventional controllers such as sky-hook controller is undertaken.

1. Introduction

Recently, the research work on vibration suppression of a vehicle system using semi-active suspension has been significantly increased. Though the passive suspension system featuring conventional oil damper provides design simplicity and cost-effectiveness, performance limitations are inevitable due to the uncontrollable damping force. On the other hand, the active suspension system can provide high control performance in wide frequency range. However, the active suspension requires high power consumption, many sensors and actuators such as servo-valve. Consequently, one way to resolve these problems is to adopt the semi-active suspension system. The semi-active suspension system offers a desirable performance generally enhanced in the active mode without requiring large power consumption and expensive hardware. For the last decade, very attractive and effective semi-active suspension system featuring an electrorheological (ER) fluid has been proposed by many investigators.

*Corresponding author. Tel.: +82 32 860 7319; fax: +82 32 868 1716.
E-mail address: seungbok@inha.ac.kr (S.-B. Choi).
URL: http://www.ssslab.com (S.-B. Choi).

0022-460X/$ - see front matter © 2007 Elsevier Ltd. All rights reserved.
doi:10.1016/j.jsv.2007.09.049

Nakano [1] proposed several semi-active control algorithms for ER damper and showed that the proportional feedback control using the information of absolute unsprung mass velocity is the most effective control strategy. Sims et al. [2] described a closed-loop control strategy which is capable of linearizing the response of an ER long-stroke damper under experimental conditions. Petek et al. [3] constructed a semi-active full suspension system consisting of four ER dampers and evaluated its effectiveness for vibration isolation. They demonstrated experimentally that unwanted pitch, heave and roll motions of vehicle body can be favorably suppressed using the simple skyhook control algorithm. Gordaninejad et al. [4] experimentally evaluated the performance of cylindrical, multi-electrode ER dampers under force vibration. They proposed simple control algorithms such as bang–bang and linear proportional controller, and experimentally demonstrated the successful implementation of the control schemes to a closed-loop system. Choi et al. [5] manufactured an ER damper for a small-sized passenger vehicle and presented its control characteristics of the damping force. On the basis of this work, they extended their research and evaluated control performance of the proposed ER damper using sliding mode controller (SMC) via hardware-in-the-loop simulation [6]. The advantage of SMC is robustness against parameter uncertainties and external disturbance and so on. In general, vehicle suspension system is easily subjected to several parameter variations such as the variation of the sprung mass. Moreover, the field-dependent time delay of the ER damper needs to be treated as an important uncertain parameter. Even though SMC is one of potential control candidates for ER suspension system, it has some limitations such as slow settling time. Moreover, the robustness of conventional SMC is not guaranteed during reaching phase. The robustness of the SMC can be improved by shortening the time required to attain the sliding mode, or may be guaranteed during whole intervals of control action by eliminating the reaching phase. One easy way to minimize the reaching phase is to employ a large control input. However, this will cause higher chattering which is undesirable in physical system, and also extreme sensitivity to unmodelled dynamics. In order to eliminate the reaching phase, Choi et al. [7] suggested a moving sliding mode controller (MSMC) and successfully implemented for uncertain control system. There are many superiorities of the MSMC such as fast tracking performance to conventional SMC. However, the MSMC proposed by Choi et al. [7] depends on exact calculations of the surface equations to make the surface function have a value in a certain range. Hence, the generalization of the MSMC to various dynamic systems is restricted by the complexity of the equations associated with moving algorithm.

Consequently, the main contribution of this study is to propose a new MSMC based on the fuzzy logic and apply to vibration control of ER suspension system. In order to accomplish this goal, a cylindrical ER damper applicable for a middle-sized vehicle is designed and manufactured, and its field-dependent damping forces are experimentally evaluated. After formulating the governing equation of motion for the quarter vehicle ER suspension system which considers the variation of the sprung mass and time delay of the ER damper as uncertain parameters, a new moving sliding mode controller based on fuzzy logic (FMSMC) is formulated by presenting moving algorithm of the sliding surface. The proposed FMSMC is then experimentally implemented in order to evaluate control performance of the quarter-car ER suspension system. Control performances under bump, sine and random road conditions are presented in time and frequency domains. In addition, in order to demonstrate the superior control performances of the proposed FMSMC to conventional control methods such as sky-hook control or SMC, a comparative work is undertaken by presenting control responses and control input fields.

2. ER suspension system

2.1. ER damper

In this work, a cylindrical type of ER damper shown in Fig. 1 is designed and manufactured. The ER damper is divided into the upper and lower chambers by the piston, and it is fully filled with the ER fluid. By the motion of the piston, the ER fluid flows through the duct between inner and outer cylinders from one chamber to the other. Thus, the operating mode of the proposed ER damper is flow mode in which two electrodes are fixed. The control voltage generated by a high voltage supply unit is connected to the inner cylinder and the ground voltage is connected to the outer cylinder. On the other hand, the gas chamber located outside of the lower chamber acts as an accumulator of the ER fluid induced by the motion of the piston.

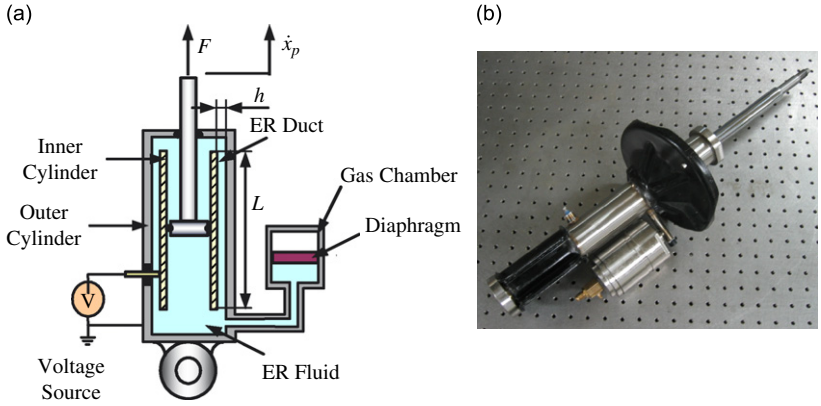

Fig. 1. The proposed ER damper for passenger vehicle: (a) schematic configuration and (b) photograph.

The proposed ER damper is applicable to a middle-sized passenger vehicle and has the following principal design parameters; electrode length $L = 292.4$ mm, electrode gap $h = 0.88$ mm, and outer cylinder radius $r = 22.5$ mm.

In the absence of the electric field, the ER damper produces damping force only caused by the fluid viscous resistance. However, if a certain level of the electric field is supplied to the ER damper, the ER damper produces additional damping force owing to the yield stress of the ER fluid. This damping force of the ER damper can be continuously tuned by controlling the intensity of the electric field. Therefore, the damping force of the proposed ER damper can be obtained as follows [6]:

$$F = k_e x_p + c_e \dot{x}_p + F_{\mathrm{ER}}, \tag{1}$$

where k_e is the effective stiffness due to the gas pressure, c_e is the effective damping due to the fluid viscosity, x_p is the excitation displacement, and F_{ER} is the field-dependent damping force which is tunable as a function of applied electric field. The controllable damping force F_{ER} can be expressed by

$$F_{\mathrm{ER}} = (A_p - A_r) 2 \frac{L}{h} \alpha E^{\beta} \mathrm{sgn}(\dot{x}_p), \tag{2}$$

where A_p and A_r represent the piston head and piston rod areas, respectively, $\mathrm{sgn}(\cdot)$ is a sign function, L is the electrode length, h is the electrode gap, and E is the electric field. The α and β are intrinsic values of the ER fluid to be experimentally determined. In this study, the field-dependent yield stress of the ER fluid is experimentally obtained to be $876.3E^{1.38}$ Pa. Here the unit of E is kV/mm.

Fig. 2 presents the measured damping force characteristics of the proposed ER damper with respect to the piston velocity at various electric fields. This is obtained by exciting the ER damper with the frequency of 3.0 Hz and the amplitude of ± 20 mm. It is clearly observed that the damping force is increased as the electric field increases. As a specific case, the damping force of 150 N at piston velocity of 0.414 m/s is increased up to 1200 N by applying the input voltage of 3.0 kV/mm. Fig. 3 shows the time response of the ER damper. It can be found that the time constant at rising case is about 19 ms, which is obtained by inspecting the required time when the damping force reaches to 63.2% of its final steady-state value. It is remarked that the time constant of the ER damper varies with respect to the intensity of the electric field, the type of ER fluid and the design parameters such as electrode length.

Fig. 4 presents the dynamic bandwidth of the damping force in frequency domain. By sweeping the input field frequencies with the magnitude of 3 kV/mm, the dynamic bandwidth is obtained. It is identified that the dynamic bandwidth of the proposed ER damper is about 28 Hz at -3 dB. Thus, both the vehicle body mode (1–2 Hz) and the wheel mode (10–15 Hz) of the passenger vehicle can be effectively controlled by employing the proposed ER damper. From the results shown in Fig. 3, the static expression of the damping force and

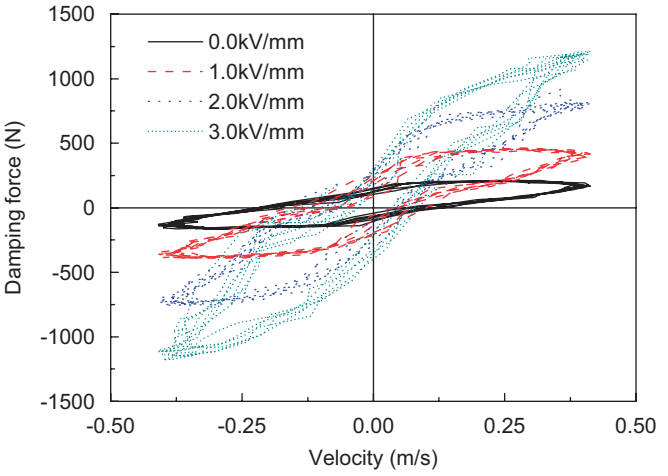

Fig. 2. The field-dependent damping force.

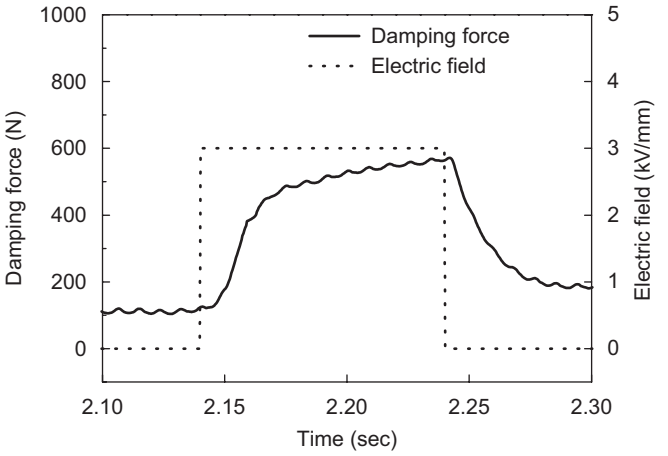

Fig. 3. Time responses of the ER damper.

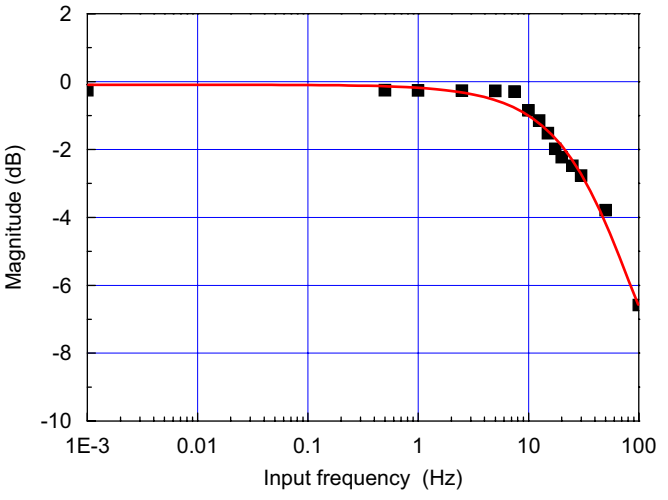

Fig. 4. Dynamic bandwidth of the ER damper in frequency domain.

input field given by Eq. (2) can be modified to take into account for the dynamic characteristics as follows:

$$\tau \frac{\mathrm{d}}{\mathrm{d}t} F_{\mathrm{ER}} + F_{\mathrm{ER}} = (A_p - A_r) 2 \frac{L}{h} \alpha E^{\beta} \operatorname{sgn}(\dot{x}_p), \tag{3}$$

where τ is the time constant of the ER damper. The dynamic model of the ER damper is to be incorporated with the suspension model.

2.2. Quarter vehicle ER suspension system

In this study, a quarter vehicle is established to evaluate control performances of the proposed ER suspension system. Fig. 5 shows the quarter vehicle model of the semi-active ER suspension system which has two degree-of-freedom. m_s and m_u represent the sprung mass and unsprung mass, respectively. The spring for the suspension is assumed to be linear and the tire is also modeled as linear spring component. Now, by considering the dynamic relationship, the state space control model is expressed for the quarter vehicle ER suspension system as follows:

$$\begin{aligned} \dot{\mathbf{x}} &= \mathbf{A}x + \mathbf{B}u + \mathbf{L}z_r, \\ \mathbf{y} &= \mathbf{C}\,\mathbf{x}, \end{aligned} \tag{4}$$

where

$$\mathbf{x} = [\, z_s \quad \dot{z}_s \quad z_u \quad \dot{z}_u \quad F_{\mathrm{ER}} \,] = [\, x_1 \quad x_2 \quad x_3 \quad x_4 \quad x_5 \,]^{\mathrm{T}},$$

$$\mathbf{A} = \begin{bmatrix} 0 & 1 & 0 & 0 & 0 \\ -\dfrac{k_s}{m_s + \Delta m_s} & -\dfrac{c_s}{m_s + \Delta m_s} & \dfrac{k_s}{m_s + \Delta m_s} & \dfrac{c_s}{m_s + \Delta m_s} & -\dfrac{1}{m_s + \Delta m_s} \\ 0 & 0 & 0 & 1 & 0 \\ \dfrac{k_s}{m_u} & \dfrac{c_s}{m_u} & -\dfrac{k_t + k_s}{m_u} & -\dfrac{c_s}{m_u} & \dfrac{1}{m_u} \\ 0 & 0 & 0 & 0 & -\dfrac{1}{\tau} \end{bmatrix},$$

$$\mathbf{B} = \begin{bmatrix} 0 & 0 & 0 & 0 & \dfrac{1}{\tau} \end{bmatrix}^{\mathrm{T}}, \quad \mathbf{C} = [\, 1 \quad 0 \quad 0 \quad 0 \quad 0 \,], \quad \mathbf{L} = \begin{bmatrix} 0 & 0 & 0 & \dfrac{k_t}{m_u} & 0 \end{bmatrix}^{\mathrm{T}},$$

$$u = (A_p - A_r) 2 \frac{L}{h} \alpha E^{\beta} \operatorname{sgn}(\dot{x}),$$

where Δm_s is the sprung mass perturbation. k_s is the total stiffness coefficient of the suspension including the effective stiffness of the ER damper in Eq. (1). c_s is the damping coefficient of the suspension and it is assumed

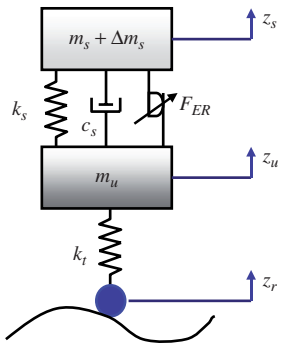

Fig. 5. Mechanical model of the quarter vehicle ER suspension system.

to be equal to c_e. In addition, k_t is the stiffness coefficient of the tire. z_s, z_u and z_r are the vertical displacement of sprung mass, unsprung mass, and excitation, respectively.

3. Controller design

The first step to formulate the SMC is to design a stable sliding surface. The stable sliding surface for the control system (4) is defined as follows:

$$s = c_1x_1 + c_2x_2 + c_3x_3 + c_4x_4 + c_5x_5, \tag{5}$$

where c_i ($i = 1$–5) are sliding surface coefficients to be determined so that the sliding surface (5) is stable. In general, the surface coefficients are fixed in the conventional SMC. In this case, the robustness of the SMC is not guaranteed during reaching phase. As noted in Introduction, the robustness of the SMC can be improved by shortening the time required to attain the sliding mode, or may be guaranteed during whole intervals of control action by eliminating the reaching phase. In order to achieve this, a moving sliding surface (MSS) associated with the rotating and shifting schemes is defined as follows [7,8]:

$$s = c_1(x_1)x_1 + c_2x_2 + c_3x_3 + c_4x_4 + c_5x_5 + \alpha(x_1). \tag{6}$$

In the above, $c_1(x_1)$ is the rotating function and $\alpha(x_1)$ is the shifting function. In the earlier work on the MSS [8], these functions have been determined on the basis of the piecewise time-constant functions. However, these piecewise functions may cause the system to be sensitive to disturbances and parameter uncertainties. In this work, in order to resolve this problem, the fuzzy tuning scheme is adopted to determine these functions.

Fig. 6 illustrates two moving patterns of the sliding surface: rotating and shifting. In this study, the rotating algorithm is applied to reduce the reaching phase of the SMC. It can change the sliding surface coefficient c_1 as a function of the displacement of the sprung mass x_1. Fig. 6(a) shows the region for possible slopes of the rotating sliding surfaces in the stable zone of the phase plane (the second and fourth quadrants). The control performance is sensitive to the slope of the sliding surface. The system will be more stable with the large slope, but control performance may be degraded because of a longer reaching time. On the other hand, the convergence speed on the sliding surface itself will be slow with the small surface coefficient c_1. In order to reduce the reaching time in the rotating algorithm, c_1 should be large when absolute value of x_1 is small and vice versa. Thus, the fuzzy rule for tuning the sliding surface coefficient c_1 can be formulated as follows:

$$\begin{aligned} &\text{If } |x_1| \text{ is larger (XL) then slope is small (CS),} \\ &\text{If } |x_1| \text{ is small (XS) then slope is large (CL).} \end{aligned} \tag{7}$$

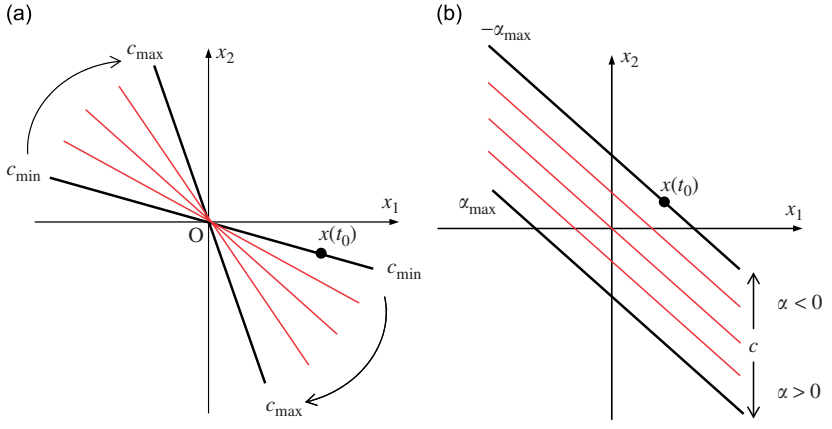

Fig. 6. Illustration of the moving sliding surface: (a) rotating sliding surface and (b) shafting sliding surface.

By defining the following membership functions [9]

$$\mu_{XS} = 2/\left[\exp(-\chi_{1r}) + \exp(\chi_{1r})\right] = 1/\cosh(\chi_{1r}),$$
$$\mu_{XL} = 1 - \mu_{XS},$$
$$\mu_{CL} = \begin{cases} 1 & \text{for } c_1 = c_{1,\max}, \\ 0 & \text{for } c_1 \neq c_{1,\max}, \end{cases} \quad \mu_{CS} = \begin{cases} 1 & \text{for } c_1 = c_{1,\min}, \\ 0 & \text{for } c_1 \neq c_{1,\min} \end{cases} \tag{8}$$

and using the centroid-method for decision-making logic, the value of the sliding surface coefficient c_1 can be found as follows (Fig. 7(a)):

$$c_1(x_1) = \frac{\mu_{XS} c_{1,\max} + \mu_{XL} c_{1,\min}}{\mu_{XS} + \mu_{XL}} = c_{1,\min} + \Delta c_1/\cosh(\chi_{1r}), \tag{9}$$

where

$$\Delta c_1 = c_{1,\max} - c_{1,\min}, \quad \chi_{1r} = x_1/\sigma_r.$$

In the above, $c_{1,\max}$ and $c_{1,\min}$ are maximum and minimum absolute values of c_1, respectively. σ_r is a certain positive constant. Therefore, we can formulate the control input of the rotating algorithm, which satisfies sliding mode condition $s \cdot \dot{s} < 0$ as follows:

$$u_r(t) = -\frac{\tau}{c_5}\left\{\left(c_1(x_1) + \frac{\Delta c_1 \chi_{1r} \sinh(\chi_{1r})}{\cosh^2(\chi_{1r})}\right)x_2 + \frac{c_2}{m_s}(-k_s x_1 - c_s x_2 + k_s x_3 + c_s x_4 - x_5) + c_3 x_4 \right.$$
$$\left. + \frac{c_4}{m_u}(k_s x_1 + c_s x_2 - (k_t + k_s)x_3 - c_s x_4 + x_5) - \frac{c_5}{\tau}x_5\right\} - k\,\mathrm{sgn}(s), \tag{10}$$

where k stands for the discontinuous gain which is a positive number, and sgn(·) stands for a signum function. By substituting Eq. (10) into Eq. (4), the sliding mode condition is satisfied as follows:

$$s \cdot \dot{s} = s(\dot{c}_1(x_1)x_1 + c_1(x_1)\dot{x}_1 + c_2\dot{x}_2 + c_3\dot{x}_3 + c_4\dot{x}_4 + c_5\dot{x}_5) = s\left\{\left(\frac{\Delta c_1 \sinh(\chi_{1r})}{\sigma_r \cosh^2(\chi_{1r})}x_2\right)x_1 + c_1(x_1)x_2\right.$$
$$+ c_2\left(\frac{-k_s x_1 - c_s x_2 + k_s x_3 + c_s x_4 - x_5}{m_s}\right) + c_3 x_4 + c_4\left(\frac{k_s x_1 + c_s x_2 - (k_t + k_s)x_3 - c_s x_4 + x_5}{m_u}\right)$$
$$\left. + c_5\left(-\frac{1}{\tau}x_5 + \frac{1}{\tau}u_r(t)\right)\right\} < 0. \tag{11}$$

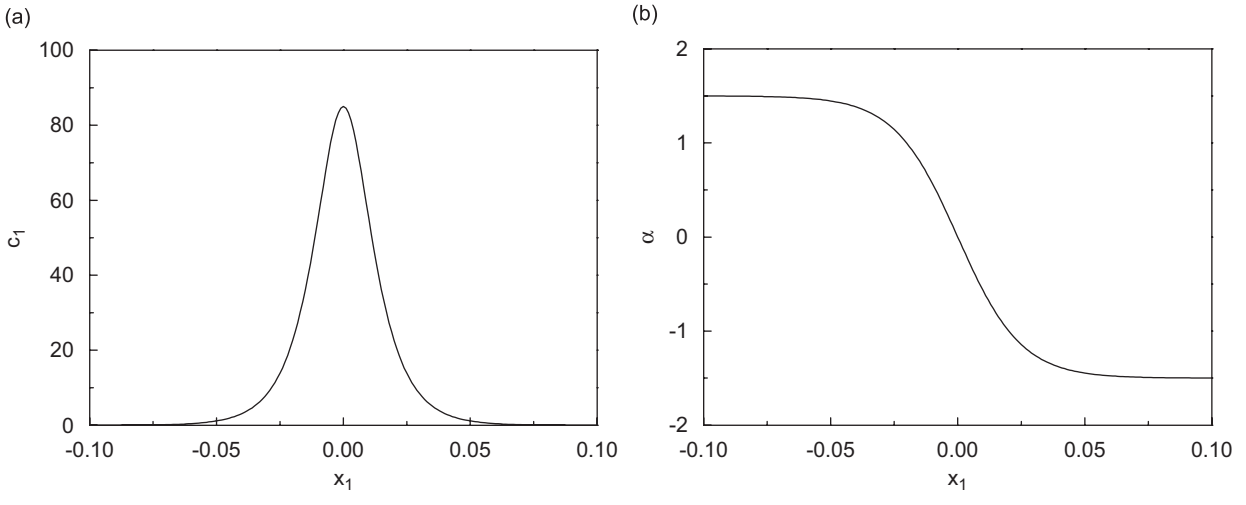

Fig. 7. Continuous functions for sliding surface: (a) sliding surface coefficient c_1 and (b) intercept α.

The robustness derived from the rotating algorithm may be absent during the reaching phase when initial conditions are located in the first and third quadrants. Hence, the shifting algorithm, which can add the intercept α as a function of x_1 in Eq. (5), is adopted and determined according to the relative place of the sliding surface. The intercept α is also tuned by the fuzzy logic according to the magnitude and sign of the sprung mass displacement x_1. Fig. 6(b) shows the possible region of the shifting sliding surfaces. If $\alpha>0$, the sliding surface is shifted increasing s and vice versa. The value for α is bounded by a constant $\alpha_{\max}$ that may be determined by the guaranteed precision for tracking. The larger the constant $\alpha_{\max}$ is, the more tolerant the tracking error can be expected. Hence, when absolute value of x_1 is large, absolute value of α should be high, and vice versa. Furthermore, the sliding surface is moved upward for positive x_1, and the sliding surface is moved downward for the opposite case. These considerations can be stated in the following fuzzy rules for tuning α:

$$\begin{aligned}&\text{If } x_1 \text{ is positive large (XPL) then intercept is negative large (INL),}\\&\text{If } x_1 \text{ is positive small (XPS) then intercept is negative small (INS)}\end{aligned} \tag{12}$$

or

$$\begin{aligned}&\text{If } x_1 \text{ is negative large (XNL) then intercept is positive large (IPL),}\\&\text{If } x_1 \text{ is negative small (XNS) then intercept is positive small (IPS).}\end{aligned}$$

By introducing the following membership functions [9]

$$\begin{aligned}&\mu_{\mathrm{XPL}}=\tanh(\chi_{1s}),\quad \mu_{\mathrm{XPS}}=1-\mu_{\mathrm{XPL}},\\&\mu_{\mathrm{INL}}=\begin{cases}1 & \text{for } \alpha=-\alpha_{\max},\\ 0 & \text{for } \alpha\neq-\alpha_{\max},\end{cases}\quad \mu_{\mathrm{INS}}=\begin{cases}1 & \text{for } \alpha=0,\\ 0 & \text{for } \alpha\neq 0\end{cases}\end{aligned} \tag{13}$$

or

$$\begin{aligned}&\mu_{\mathrm{XNL}}=-\tanh(\chi_{1s}),\quad \mu_{\mathrm{XNS}}=1-\mu_{\mathrm{XNL}},\\&\mu_{\mathrm{IPL}}=\begin{cases}1 & \text{for } \alpha=\alpha_{\max},\\ 0 & \text{for } \alpha\neq\alpha_{\max},\end{cases}\quad \mu_{\mathrm{IPS}}=\begin{cases}1 & \text{for } \alpha=0,\\ 0 & \text{for } \alpha\neq 0\end{cases}\end{aligned}$$

and using the centroid-method for decision-making logic, the value of α can be found as follows (Fig. 7(b)):

$$\alpha(x_1)=\frac{\mu_{\mathrm{XPL}}\alpha_{\max}}{\mu_{\mathrm{XPL}}+\mu_{\mathrm{XPS}}}=\frac{\mu_{\mathrm{XNL}}\alpha_{\max}}{\mu_{\mathrm{XNL}}+\mu_{\mathrm{XNS}}}=-\alpha_{\max}\tanh(\chi_{1s}), \tag{14}$$

where

$$\chi_{1s}=x_1/\sigma_s$$

in the above, σ_s is some positive constant. Therefore, we can formulate the control input of the shifting algorithm, which satisfies sliding mode condition $s\cdot\dot{s}<0$ as follows:

$$\begin{aligned}u_s(t)=-\frac{\tau}{c_5}\Bigg\{&\left(c_1(x_1)-\frac{(\alpha_{\max}/\sigma_s)}{\cosh^2(\chi_{1s})}\right)x_2+\frac{c_2}{m_s}(-k_sx_1-c_sx_2+k_sx_3+c_sx_4-x_5)\\&+c_3x_4+\frac{c_4}{m_u}(k_sx_1+c_sx_2-(k_t+k_s)x_3-c_sx_4+x_5)-\frac{c_5}{\tau}x_5\Bigg\}-k\,\mathrm{sgn}(s).\end{aligned} \tag{15}$$

By substituting Eq. (15) into Eq. (4), the sliding mode condition is satisfied as follows:

$$\begin{aligned}s\cdot\dot{s}&=s(c_1\dot{x}_1+c_2\dot{x}_2+c_3\dot{x}_3+c_4\dot{x}_4+c_5\dot{x}_5+\dot{\alpha}(x_1))\\&=s\Bigg\{\left(c_1-\frac{(\alpha_{\max}/\sigma_s)}{\cosh^2(\chi_{1s})}\right)x_2+c_2\left(\frac{-k_sx_1-c_sx_2+k_sx_3+c_sx_4-x_5}{m_s}\right)+c_3x_4\\&\quad+c_4\left(\frac{k_sx_1+c_sx_2-(k_t+k_s)x_3-c_sx_4+x_5}{m_u}\right)+c_5\left(-\frac{1}{\tau}x_5+\frac{1}{\tau}u_s(t)\right)\Bigg\}<0.\end{aligned} \tag{16}$$

Consequently, we can formulate the control input of the proposed FMSMC, which is combined the rotating algorithm (10) and shifting algorithm (15), and satisfies sliding mode condition $s \cdot \dot{s} < 0$ as follows:

$$u(t) = -\frac{\tau}{c_5}\left\{\left(c_1(x_1) + \frac{\Delta c_1 \chi_{1r} \sinh(\chi_{1r})}{\cosh^2(\chi_{1r})} - \frac{(\alpha_{\max}/\sigma_s)}{\cosh^2(\chi_{1s})}\right)x_2 + \frac{c_2}{m_s}(-k_s x_1 - c_s x_2 + k_s x_3 + c_s x_4 - x_5)\right.$$
$$\left. + c_3 x_4 + \frac{c_4}{m_u}(k_s x_1 + c_s x_2 - (k_t + k_s)x_3 - c_s x_4 + x_5) - \frac{c_5}{\tau}x_5\right\} - k\,\mathrm{sgn}(s). \tag{17}$$

Since the controller u includes the signum function, undesirable chattering may occur during control action. Therefore, by replacing the signum function to the saturation function with appropriated boundary layer thickness, we can attenuate the undesirable chattering problem [10].

Fig. 8 presents the block diagram of the proposed FMSMC. The basic configuration of the fuzzy control (FC) consists of three components: a fuzzification interface, a decision-making logic and a defuzzification interface. In the fuzzification interface, x_1 is modified into membership functions μ. In the decision-making logic based on the centroid-method and the defuzzification interface, the fuzzy output c_1 and α are decided for the purpose of real control input. The control input determined from the FMSMC controller is to be applied to the ER damper depending upon the motion of suspension travel. Therefore, the following semi-active actuating condition is normally imposed:

$$u = \begin{cases} u & \text{for } u(\dot{z}_s - \dot{z}_u) > 0, \\ 0 & \text{for } u(\dot{z}_s - \dot{z}_u) \leqslant 0. \end{cases} \tag{18}$$

The above condition physically implies that the activating of the controller u only assures the increment of energy dissipation of the stable system. Once the control input u is determined, the input electric field to be applied to the ER damper is obtained by

$$E = \left[u\frac{h}{2\alpha L(A_p - A_r)}\right]^{1/\beta}. \tag{19}$$

4. Experimental results and discussion

From the practical point of view, the ER suspension system should be installed on the full vehicle and its effectiveness for the ride quality needs to be evaluated under various road conditions. However, it is very expensive to completely build the entire full-vehicle system with hardware from the start. Therefore, we adopt a quarter vehicle system, which is well corresponding with the field test. An experimental apparatus for the quarter vehicle test is established as shown in Fig. 9 to evaluate control performance of the ER suspension

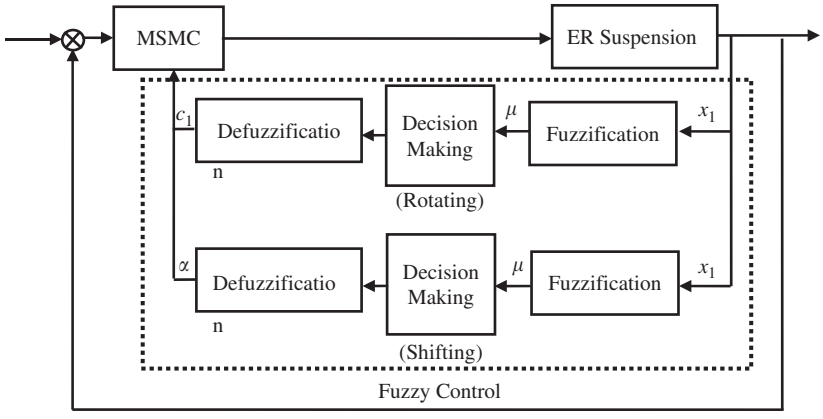

Fig. 8. Block-diagram of the proposed FMSMC.

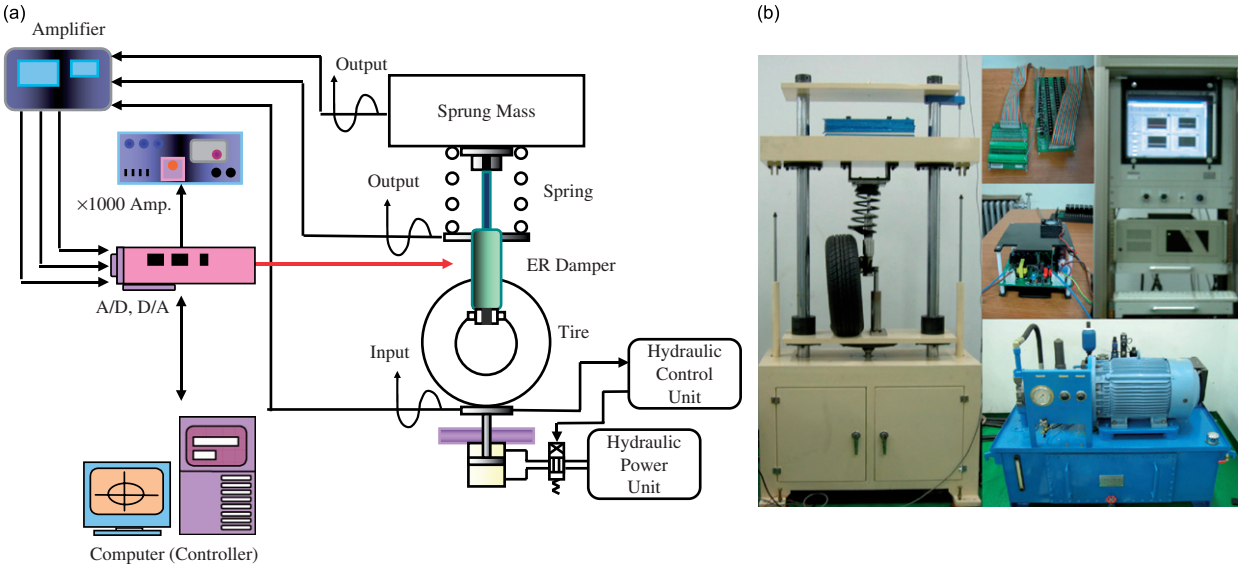

Fig. 9. Experimental setup for the quarter vehicle ER suspension system: (a) schematic diagram and (b) photograph.

Table 1
System parameters of a quarter vehicle ER suspension system

Parameter	Value
m_s	310 kg
m_u	70 kg
k_s	27,358 N/m
k_t	309,511 N/m
c_s	984 N s/m
A_p	0.00080 m^2
A_r	0.00038 m^2
L	0.2924 m
h	0.00088 m

system proposed in this work. The ER damper, sprung mass, spring and tire are installed on the hydraulic system and the sprung mass displacement and suspension travel are measured by two LVDT displacement sensors. The hydraulic system applies the displacement (suspension travel) to the ER suspension system according to the demand signal obtained from the computer. It is also connected to the voltage amplifier which applies control voltage determined from control algorithm to the ER damper. The system parameters of the quarter vehicle ER suspension system are chosen on the basis of the conventional suspension system for a middle-sized passenger vehicle, and listed in Table 1. It is noted that the state observer to estimate the states x_1–x_4 can be used in order to realize the proposed FMSMC in vehicle applications.

In this study, control characteristics of the quarter vehicle ER suspension system were evaluated under three types of excitation (road) conditions. The first excitation, normally used to reveal the transient response characteristic is a bump described by

$$z_r = z_b[1 - \cos(\omega_r t)], \tag{20}$$

where $\omega_r = 2\pi V/D$. z_b is the half of the bump height (0.035 m), D is the width of the bump (0.8 m). In the bump excitation, the vehicle travels the bump with constant vehicle velocity of 3.08 km/h (= 0.856 m/s).

The second type is a sinusoidal function described by

$$z_r = z_e \sin \omega t, \tag{21}$$

where ω is the excitation frequency (0.5–15 Hz) and z_e is the excitation level (0.01 m). In general, by using the sinusoidal function as the excitation for the quarter vehicle suspension system, overall frequency responses can be simply obtained for the interesting frequency range. The third type of road excitation, normally used to evaluate the frequency response, is a stationary random process [11] with zero mean described by

$$\dot{z}_r + \rho_r V z_r = V W_n, \tag{22}$$

where W_n is the white noise with intensity $2\sigma^2\rho_r V$. ρ_r is the road roughness parameter, and σ^2 is the covariance of road irregularity. In random excitation, the values of road irregularity are chosen by assuming that the vehicle travels on the paved road with the constant velocity of 72 km/h (= 20 m/s). The values of $\rho_r = 0.45\,\mathrm{m}^{-1}$ and $\sigma^2 = 300\,\mathrm{mm}^2$ are chosen in the sense of the paved road condition.

Figs. 10–13 present time responses of the ER suspension system under the bump excitation. In this study, it is assumed that the sprung mass without any additional mass is the nominal value ($m_s = 310$ kg) for the proposed control system. On the other hand, in order to investigate the robustness of the proposed FMSMC, the sprung mass is added to the mass of a driver by 70 kg for perturbed quarter vehicle system. As shown in Fig. 10(a), it is obvious that unwanted vibrations induced from the bump excitation have been well reduced by adopting the skyhook controller, SMC and the proposed FMSMC to the ER suspension system. However, from the magnification of the settling responses shown in Fig. 10(b) it is clearly seen that the FMSMC proposed in this work gives the fastest settling response without increasing the control electric field (refer to Fig. 11). This is mainly due to that reaching phase can be decreased by applying the FMSMC. It is noted here that electric field is limited at 3.5 kV/mm for safety. Figs. 12 and 13 show bump responses of the proposed system with parameter perturbations. As clearly observed from the results the vertical displacement was well reduced by employing the control electric field determined from the proposed FMSMC even in the presence of parameter perturbations. Fig. 14 presents the variations of the sliding surface s during control action of the SMC and FMSMC under the bump excitation. It is clearly seen that the sliding surface of FMSMC is effectively changed in order to reduce the reaching phase after 2.0 s. By employing the proposed FMSMC, the reaching time in case of sprung mass 310 kg is decreased from 2.147 to 2.133 s, while the reaching time in case of sprung mass 380 kg is decreased from 2.271 to 2.217 s. Fig. 15 presents the variations of the sliding surface coefficients c_1 and intercept α during control action of the FMSMC under the bump excitation. It is clearly seen that the sliding surface coefficients are effectively changed in order to reduce the reaching phase depending upon the sprung mass displacement.

Fig. 16(a) presents the frequency domain responses of the ER suspension system without parameter perturbations. The frequency responses were obtained from transmissibility of the suspension travel ($z_s - z_u$). The root mean square (rms) values of input and output are used to obtain the transmissibility. As expected,

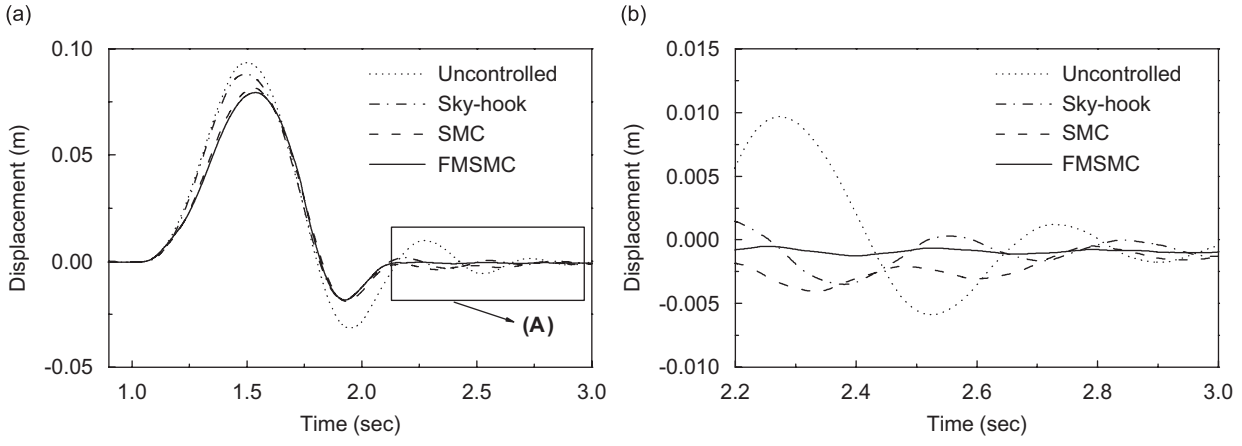

Fig. 10. Comparison of bump response with the sprung mass—310 kg: (a) displacement of the sprung mass and (b) magnification of (A).

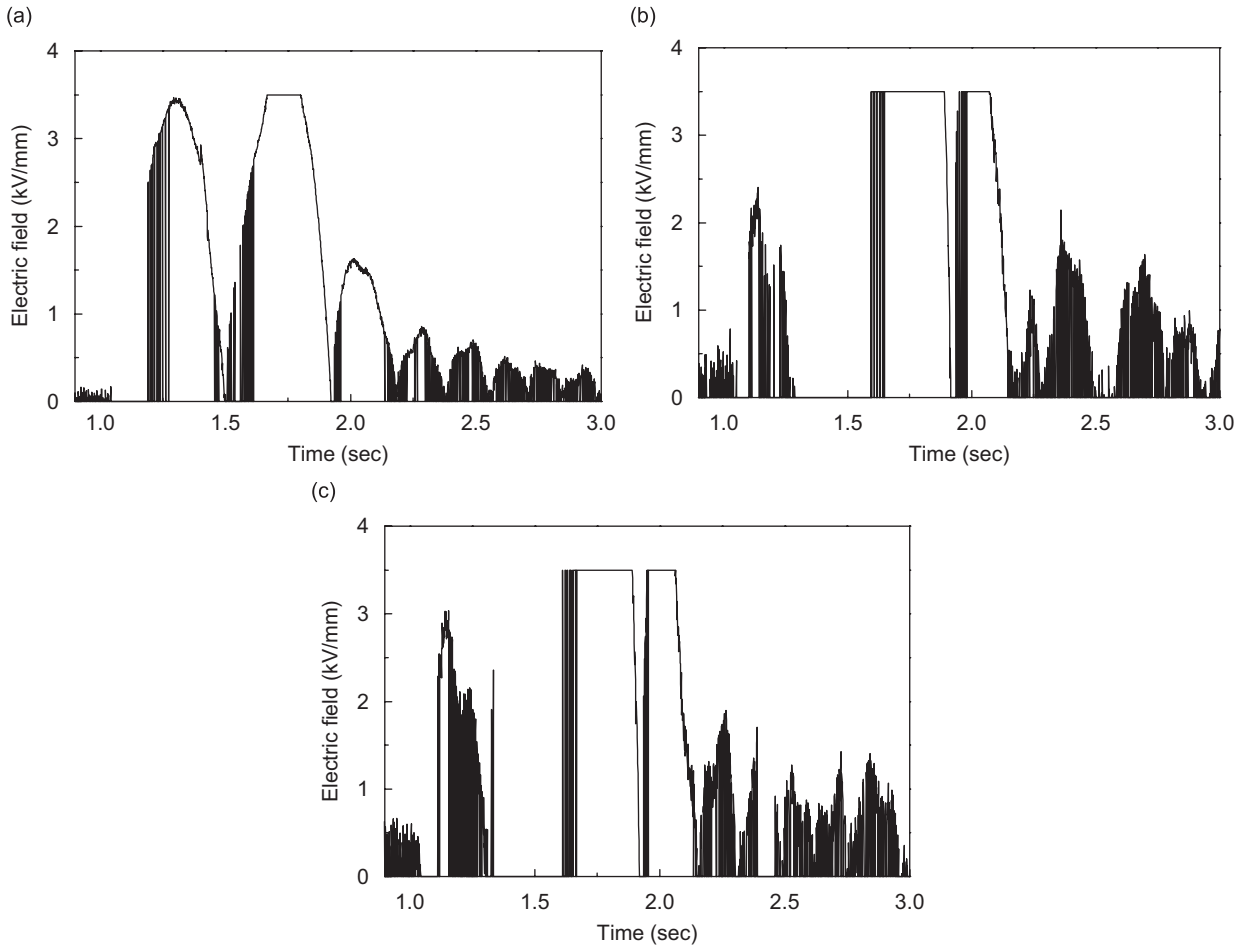

Fig. 11. Comparison of control electric field with the sprung mass—310 kg: (a) skyhook, (b) SMC and (c) FMSMC.

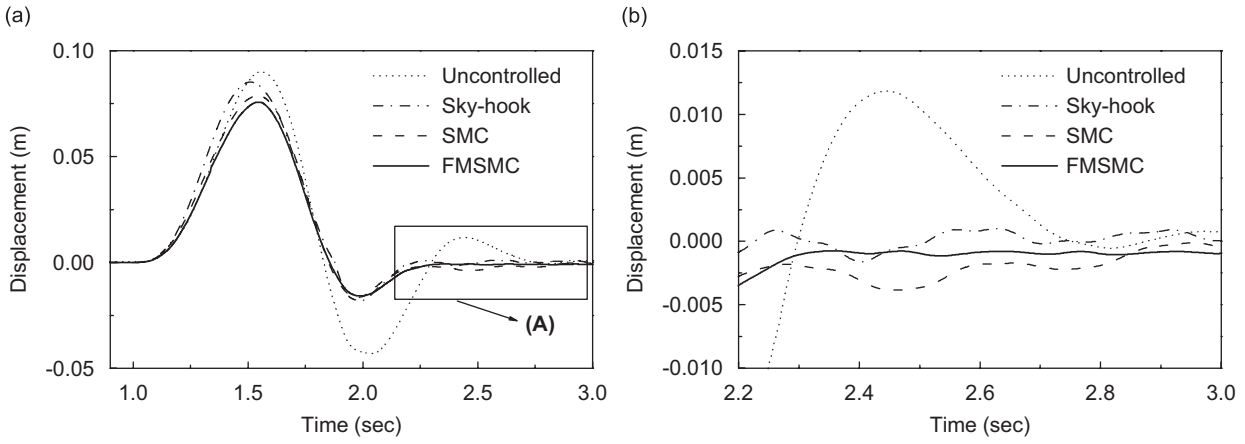

Fig. 12. Comparison of bump response with the sprung mass—380 kg: (a) displacement of the sprung mass and (b) magnification of (A).

the transmissibility of the suspension travel has been substantially reduced in the neighborhood of body resonance (1–2 Hz). In addition, it can be found that the wheel resonance (10–15 Hz) exists in the transmissibility of the suspension travel because it is the relative displacement between sprung mass (body)

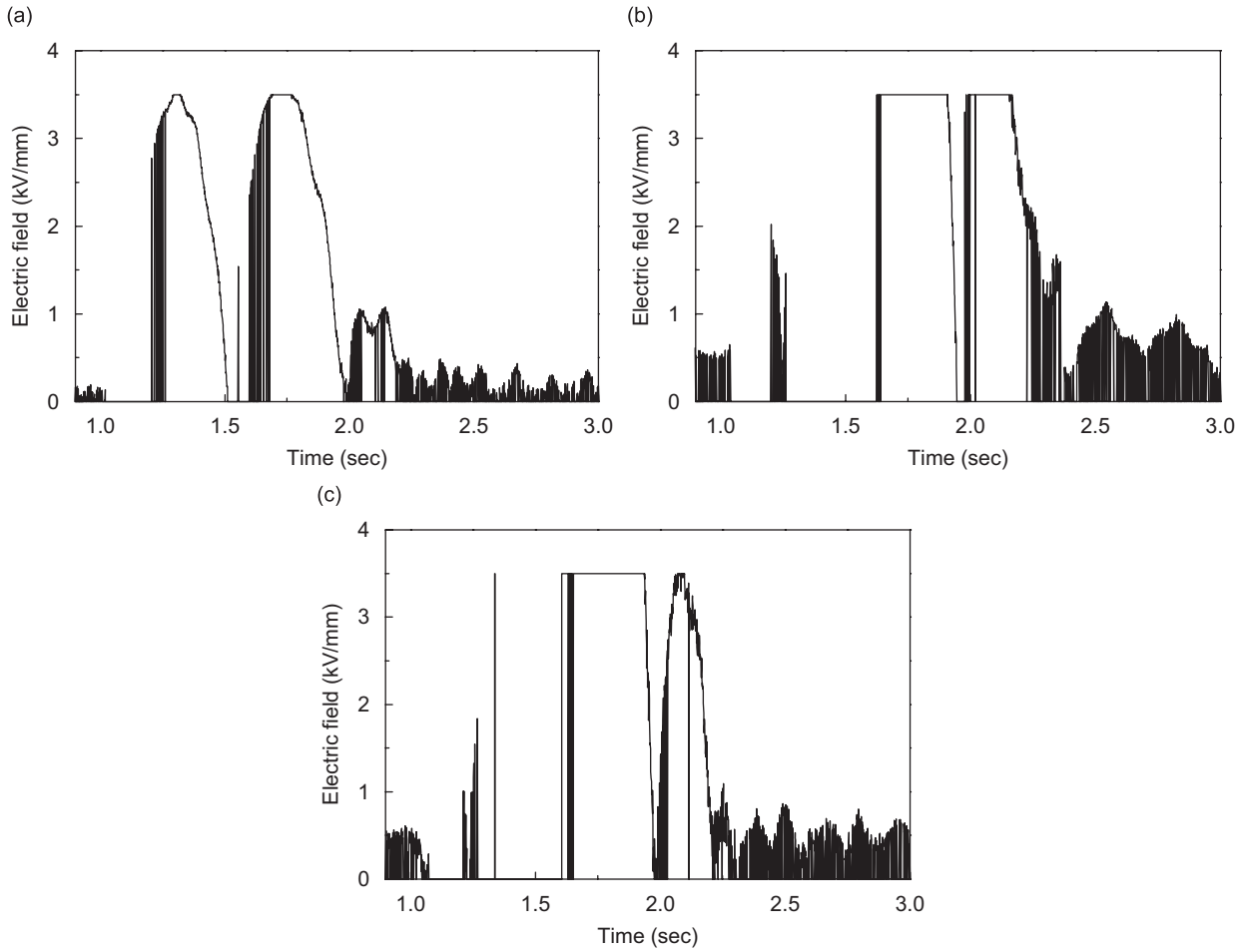

Fig. 13. Comparison of control electric field with the sprung mass—380 kg: (a) skyhook, (b) SMC and (c) FMSMC.

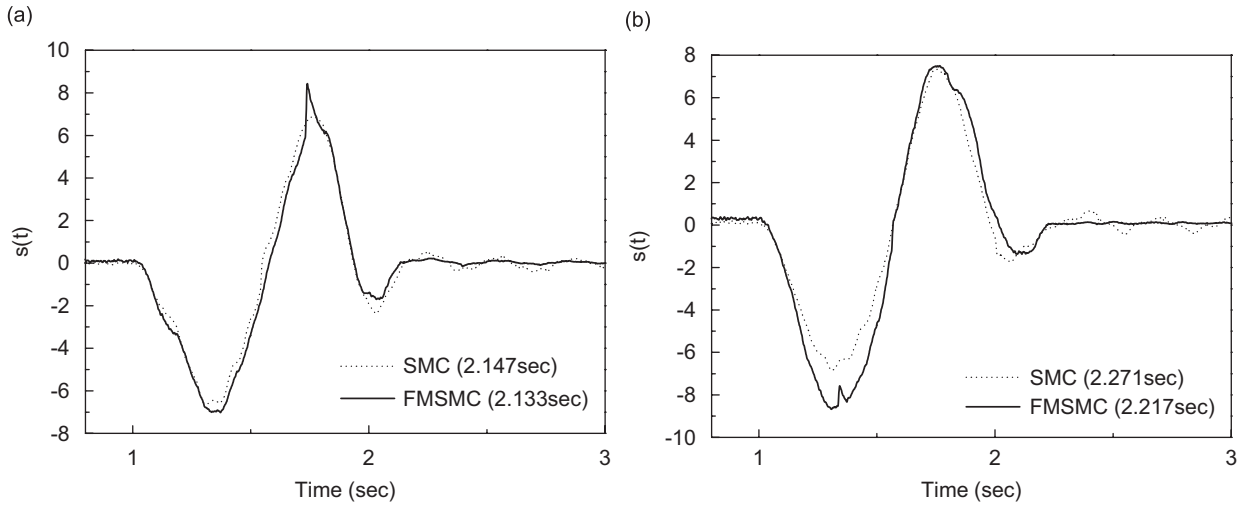

Fig. 14. Variations of sliding surface under bump excitation: (a) sprung mass 310 kg and (b) sprung mass 380 kg.

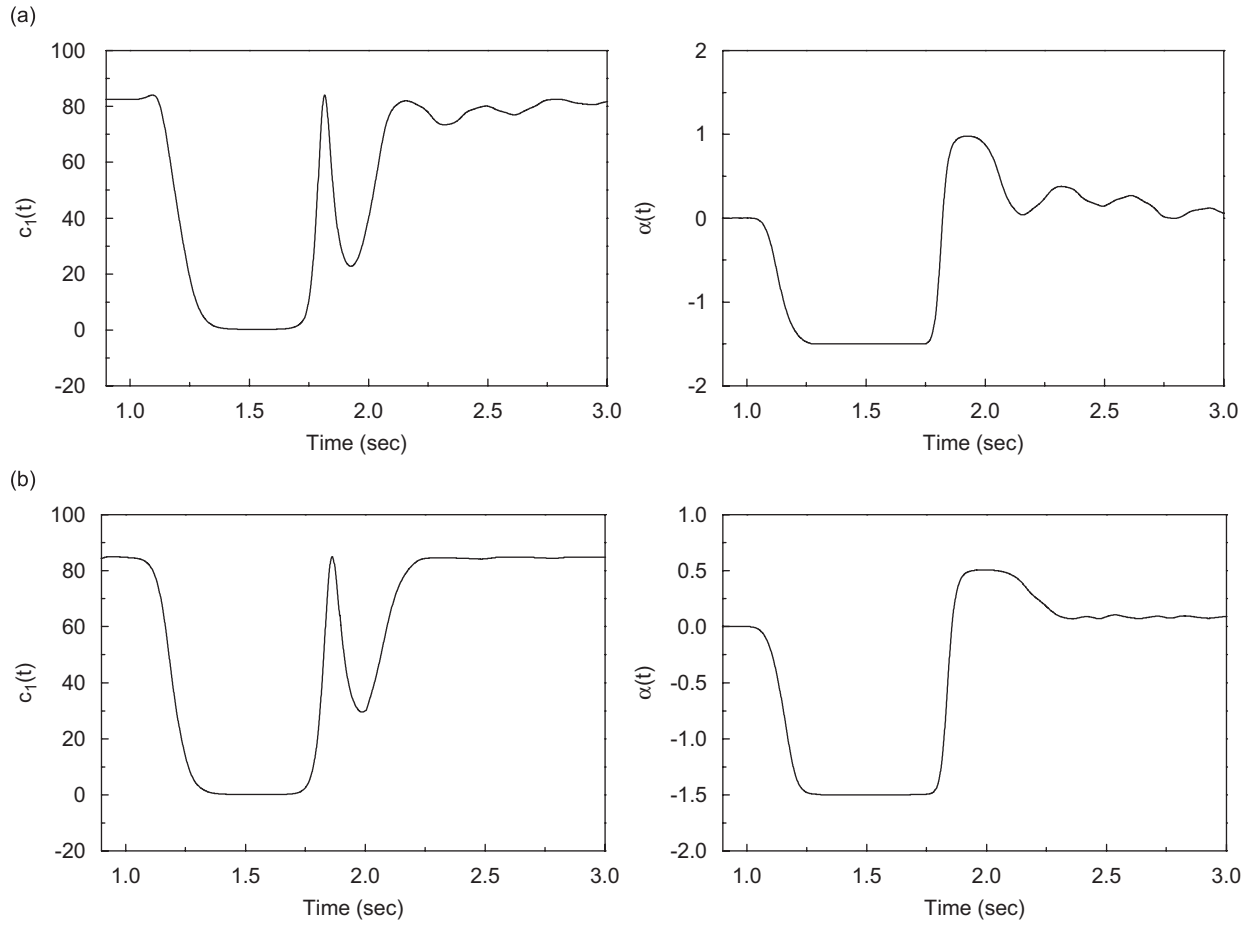

Fig. 15. Variations of sliding surface coefficients under bump excitation: (a) sprung mass 310 kg and (b) sprung mass 380 kg.

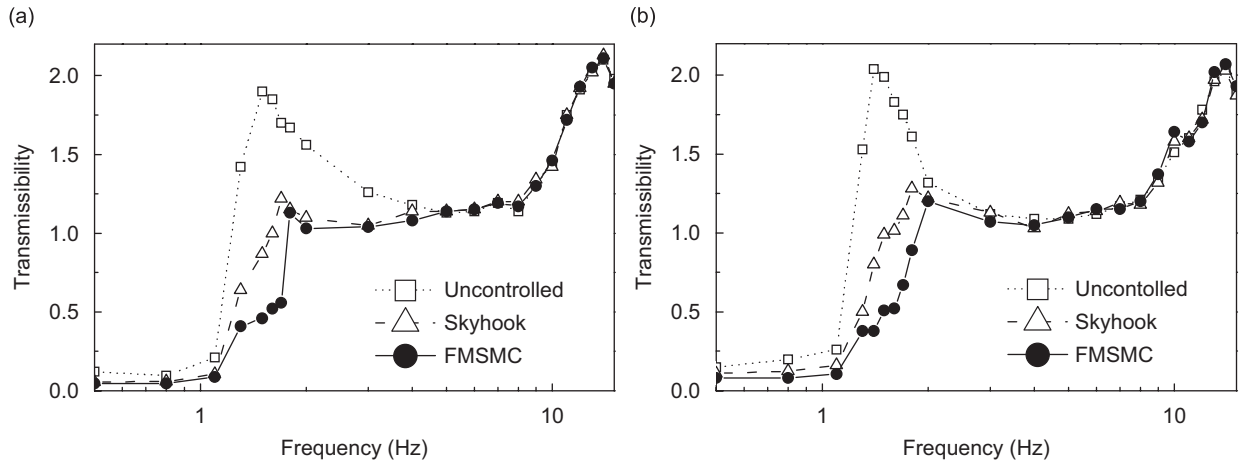

Fig. 16. Sinusoidal responses of the ER suspension system: (a) sprung mass 310 kg and (b) sprung mass 380 kg.

and unsprung mass (wheel). As well known, the driving stability is mainly affected by the vibration of the wheel. Therefore, we can obtain favorable driving stability by reducing the magnitude of the wheel vibration. However, it is hard to simultaneously meet both good ride comfort and driving safety since there exists a

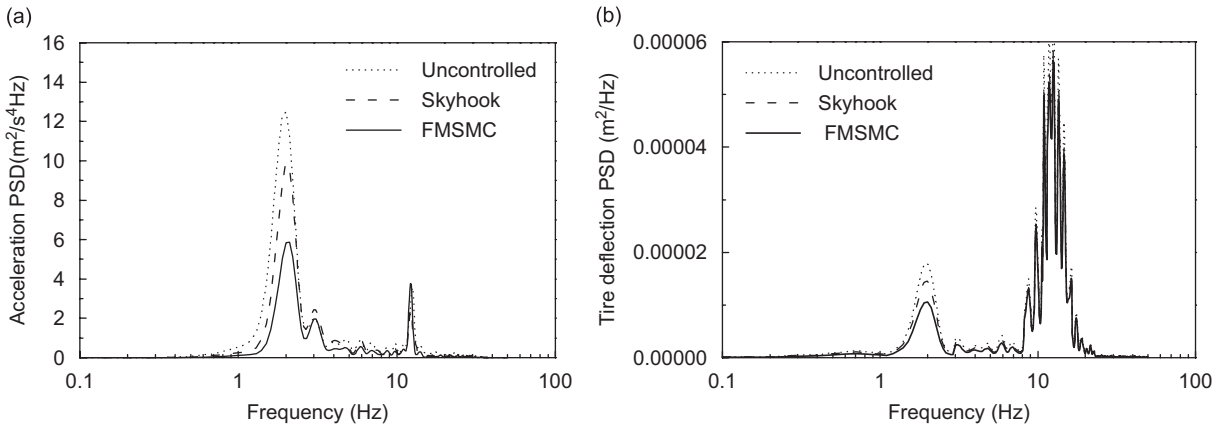

Fig. 17. Random road responses of the ER suspension system—310 kg: (a) vertical acceleration and (b) tire deflection.

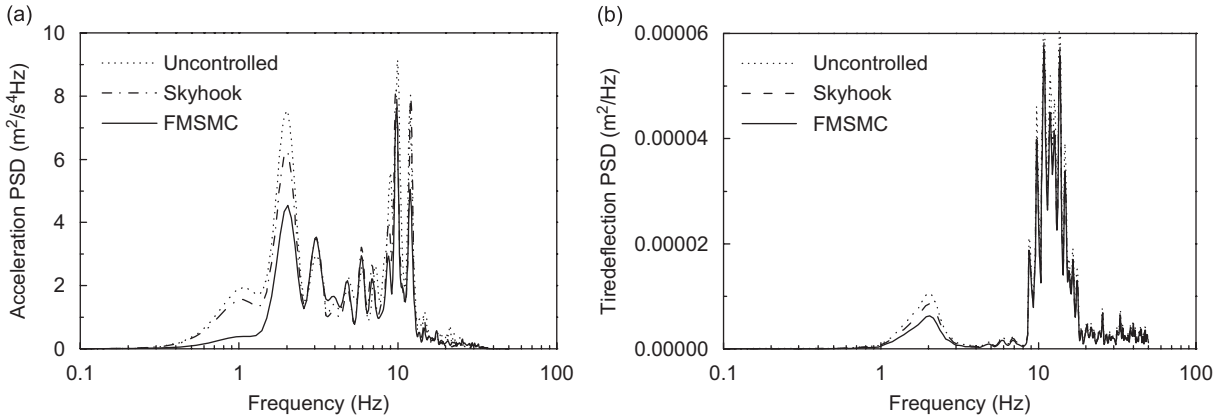

Fig. 18. Random road responses of the ER suspension system—380 kg: (a) vertical acceleration and (b) tire deflection.

trade-off between these two objectives. In this study, the wheel resonance control is not considered. It is noted that using the filter-integrated control algorithms [12], both body and wheel resonance can be effectively reduced and it is going to be undertaken in the our next research scope. Fig. 16(b) presents the frequency domain responses of the ER suspension system with parameter perturbations. It is clearly seen that frequency response at body resonance was well reduced by adopting the proposed FMSMC although the parameter perturbations exist.

Figs. 17 and 18 present controlled frequency responses using the proposed FMSMC under random road excitation without and with perturbations, respectively. The frequency responses are obtained from power spectral density (PSD) of the vertical acceleration of the sprung mass. As expected, the PSD of the vertical acceleration has been considerably reduced in the neighborhood of body resonance (1–2 Hz) by applying control input. The control results presented in Figs. 10–18 indicate that ride comfort of a vehicle system can be substantially improved by employing the ER suspension system associated with the proposed FMSMC.

5. Conclusion

Vibration control performance of the electrorheological (ER) suspension system for a passenger vehicle was evaluated by adopting fuzzy moving sliding mode controller (FMSMC). A cylindrical ER damper was designed and manufactured. After evaluating the field-dependent damping characteristics of the ER damper, a quarter vehicle suspension system was then constructed and its governing equations of motion were derived.

In order to obtain a favorable control performance of the ER suspension system subjected to parameter perturbations, FMSMC was designed and experimentally realized to quarter vehicle ER suspension system. It has been experimentally shown that the FMSMC can reduce the settling response under bump excitation by reducing the reaching phase. In addition, it has been demonstrated that using the proposed control methodology vibration levels such as sprung mass acceleration can be significantly reduced at body resonance region. This directly indicates that ride comfort of the vehicle system can be substantially improved by adopting the ER suspension system associated with the proposed control strategy.

Acknowledgement

This work was supported by Inha University Research Grant. This financial support is gratefully acknowledged.

References

[1] M. Nakano, A novel semi-active control of automotive suspension using an electrorheological shock absorber, *Proceedings of the Fifth International Conference on ER Fluid, MR Suspensions and Associated Technology*, Sheffield, 1995, pp. 645–653.
[2] N.D. Sims, R. Stanway, S.B.M. Beck, Proportional feedback control of an electro-rheological vibration damper, *Journal of Intelligent Material Systems and Structures* 8 (1997) 426–433.
[3] N.K. Petek, D.J. Romstadt, M.B. Lizell, T.R. Weyenberg, Demonstration of an automotive semi-active suspension using electrorheological fluid, SAE Technical Paper Series 950586, 1995.
[4] F. Gordaninejad, A. Ray, H. Wang, Control of forced vibration using multi-electrode electro-rheological fluid dampers, *ASME Journal of Vibration and Acoustics* 119 (1997) 527–531.
[5] S.B. Choi, Y.T. Choi, E.G. Chang, S.J. Han, C.S. Kim, Control characteristics of a continuously variable ER damper, *Mechatronics* 8 (1998) 143–161.
[6] S.B. Choi, Y.T. Choi, D.W. Park, A sliding mode control of a full-car electrorheological suspension system via hardware-in-the-loop simulation, *ASME Journal of Dynamics, Measurement and Control* 122 (2000) 114–121.
[7] S.B. Choi, C.C. Cheong, D.W. Park, Moving switching surfaces for robust control of second-order variable structure systems, *International Journal of Control* 58 (1993) 229–247.
[8] D.W. Park, S.B. Choi, Moving sliding surface for high-order variable structure systems, *International Journal of Control* 72 (1999) 960–970.
[9] C.C. Lee, Fuzzy logic in control systems: fuzzy logic controller—part I, II, *IEEE Transactions of Systems, Man, and Cybernetics* 20 (1990) 404–435.
[10] J.J.E. Slotine, W. Li, *Applied Nonlinear Control*, Prentice-Hall, Englewood Cliffs, NJ, 1991.
[11] N.C. Nigam, S. Narayanan, *Applications of Random Vibrations*, Springer, New York, 1994.
[12] M. Lizell, Dynamic leveling a low power active suspension with adaptive control, *ImechE Conference*, 1993, pp. 385–400.